

# Cellulose Nanopaper Structures of High Toughness

Marielle Henriksson,<sup>†</sup> Lars A. Berglund,<sup>\*,†</sup> Per Isaksson,<sup>‡</sup> Tom Lindström,<sup>§</sup> and Takashi Nishino<sup>||</sup>

*Fibre and Polymer Technology, Royal Institute of Technology, KTH, SE-100 44 Stockholm, Sweden, Solid Mechanics, Mid Sweden University/FSCN, 85170 Sundsvall, Sweden, STFI-Packforsk AB, Box 5604, SE-114 86 Stockholm, Sweden, and Chemical Science and Engineering, Faculty of Engineering, Kobe University, Rokko, Nada, Kobe 657-8501, Japan*

Received January 14, 2008; Revised Manuscript Received March 13, 2008

Cellulose nanofibrils offer interesting potential as a native fibrous constituent of mechanical performance exceeding the plant fibers in current use for commercial products. In the present study, wood nanofibrils are used to prepare porous cellulose nanopaper of remarkably high toughness. Nanopapers of different porosities and from nanofibrils of different molar mass are prepared. Uniaxial tensile tests are performed and structure–property relationships are discussed. The high toughness of highly porous nanopaper is related to the nanofibrillar network structure and high mechanical nanofibril performance. Also, molar mass correlates with tensile strength. This indicates that nanofibril fracture controls ultimate strength. Furthermore, the large strain-to-failure means that mechanisms, such as interfibril slippage, also contributes to inelastic deformation in addition to deformation of the nanofibrils themselves.

## Introduction

Cellulose is the main reinforcing constituent in plant cell walls. It is present in the form of aligned poly- $\beta$ (1,4)-D-glucan molecules in extended chain conformation assembled into microfibrils of high modulus<sup>1</sup> and tensile strength.<sup>2</sup> Microfibrils have a lateral dimension of typically 5–10 nm, depending on plant source, and are several micrometers in length. Often, cellulose materials are based on plant cells, for instance in the form of wood pulp. Despite good inherent properties of cellulose, the use of materials and products from cellulose tends to be motivated by low cost. Even in light of the recent interest in biocomposite materials, cellulose tends to be viewed as “filler” and it usually embrittles the polymer matrix.<sup>3</sup> This disadvantage is balanced by its availability as a low cost constituent obtainable from renewable resources. However, to fully realize the potential of cellulose, it is promising to utilize it as a nanostructured high-performance constituent in the form of nanofibrils.

The importance of cellulose nanofibril network formation was first demonstrated in polymer nanocomposites.<sup>4,5</sup> Nanocomposites were prepared from a water suspension of cellulose nanofibrils (tunicate whiskers) and a water-based thermoplastic latex. Favier et al. demonstrated that the addition of as little as 6% tunicate whiskers is sufficient to form a network that will strongly increase the storage modulus above the glass transition temperature.<sup>4,5</sup> Tunicate whiskers have high modulus and form strong interfibrillar bonds between ordered cellulose surfaces so that the network provides substantial stiffening to the rubbery matrix. Several reviews have been published on the subject of cellulose nanocomposites.<sup>6,7</sup>

The first studies on cellulose nanocomposites of high cellulose content are published by Nakagaito and Yano.<sup>8</sup> A porous

network of microfibrillated cellulose from wood pulp is impregnated by liquid low molar mass polyphenol formaldehyde (PF) precursors and the liquid is polymerized. The materials show high modulus and strength but are quite brittle. Materials based on melamine-formaldehyde show similar brittleness.<sup>9</sup> However, ref 8 illustrates that cellulose nanofibril networks have potential as high-performance materials and not only as low cost biocomposites. This impression is strengthened by the use of nanostructured cellulose networks in biomedical applications<sup>10,11</sup> and in transparent materials for high-technology applications.<sup>12</sup>

In our laboratory, we have prepared cellulose nanofibrils from wood pulp.<sup>13</sup> The pulp fibers are subjected to pretreatment by a combination of enzymatic hydrolysis and mechanical beating. This is an environmentally friendly way to facilitate subsequent nanofibril disintegration from the cell wall by mechanical homogenization. The enzyme treatment can also be carried out at quite low enzyme concentration.<sup>14</sup> The subsequent procedure for mechanical homogenization disintegrates the cell wall into nanofibrils by subjecting dilute wood fiber suspensions to high shear forces. The homogenization method to produce microfibrillated cellulose was originally developed by Herrick et al.<sup>15</sup> and Turbak et al.<sup>16</sup> Recently, we studied nanocomposites consisting of a wood cellulose nanofibril network in a plasticized potato starch matrix.<sup>17</sup> In an earlier study, this material showed favorable cellulose nanofibril–matrix interactions.<sup>18</sup> We furthermore discovered that this type of cellulose–starch nanocomposite can show very high toughness (work to fracture) in uniaxial tensile loading.<sup>17</sup> Because the matrix in question is highly plasticized (50% glycerol), the mechanical integrity depends strongly on the cellulose nanofibril network. The network itself is, therefore, a conceptually important material structure and worthy of further study.

In the present work, the objective is to prepare and study cellulose nanopaper structures. In particular, the porous nature of the nanofibril network is not discussed much in previous literature. The preparation is an environmentally friendly route starting from nanofibril–water suspensions, where the water is removed so that a cellulose nanofibril network is formed.

\* To whom correspondence should be addressed. Phone: +46-8-7908118. Fax: +46-8-7908101. E-mail: blund@kth.se.

<sup>†</sup> Royal Institute of Technology.

<sup>‡</sup> Mid Sweden University/FSCN.

<sup>§</sup> STFI-Packforsk AB.

<sup>||</sup> Kobe University.

Cellulose nanofibrils of different average molar mass are used, and liquids other than water are introduced so that the porosity can be varied in the films. Uniaxial tensile tests are performed and structure–property relationships are interpreted and deformation mechanisms are of particular interest.

Interestingly, the high molar mass nanofibrils form nanopaper structures of much higher toughness than previously reported in the literature for networks based on microfibrillated cellulose (MFC) from wood fibers<sup>9,19–22</sup> from parenchyma cells<sup>23–25</sup> and from bacterial cellulose (BC).<sup>26,27</sup>

## Experimental Section

**Preparation of MFC.** The different kinds of microfibrillated cellulose (MFC) used in this study are termed DP-X, where X corresponds to the average degree of polymerization (DP) of the specific MFC sample, estimated from viscosity data, see later in this section.

The MFC was prepared from softwood dissolving pulp kindly provided by Domsjö Fabriker AB, Sweden. The pulp was subjected to a pretreatment step followed by disintegration into MFC by a homogenization process with a Microfluidizer M-110EH, Microfluidics Inc., U.S.A. The pretreatment is carried out in 40 g batches. There is no upper limit for the amount that can be processed in the Microfluidizer (flow speed is about 400 mL/min). In the pretreatment step, the pulp is subjected to a combination of enzymatic degradation and mechanical beating in a laboratory beater. The enzyme used is an endoglucanase, Novozym 476, manufactured by Novozymes A/S, Denmark, believed to preferably degrade cellulose in disordered regions. This MFC preparation is based on the method explained in detail by Henriksson et al.<sup>13</sup> with a few modifications. During the enzymatic treatment, a phosphate buffer prepared from 11 mM NaH<sub>2</sub>PO<sub>4</sub> and 9 mM Na<sub>2</sub>HPO<sub>4</sub> with pH 7 was used. The fibers were incubated at 50 °C for 2 h, washed, and thereafter incubated at 90 °C to stop the enzyme activity. Different concentrations of enzymes used in the pretreatment step correspond to different degrees of polymerization for the resulting MFC. The enzyme concentrations used were 5, 5, and 0.2 μL per gram pulp fibers. This resulted in MFC with average DP of 410, 580, and 820, respectively. The reason why the same concentration, 5 μL per gram pulp fibers, resulted in two different average DPs is that for the DP 410 case, the enzyme activity was not stopped immediately after incubation.

After pretreatment, the pulp was passed 12 times through the microfluidizer to produce cellulose nanofibrils. During the first three passes, chambers with dimensions of 400 μm (first chamber) and 200 μm (second chamber) were used. The pressure was 950 bar. During the nine last passes, chambers with dimensions of 200 μm (first) and 100 μm (second) were used. During these passes, the pressure was 1650 bar. The MFCs termed DP-410, DP-580, and DP-820 are prepared by this method.

DP-800 was delivered from STFI-Packforsk and is prepared by a similar method as above. The pulp used was bleached sulfite softwood (Domsjö ECO Bright), which has higher hemicellulose content than the dissolving pulp. Details on the specific preparation method for this sample are reported by Pääkkö et al.<sup>14</sup> DP-1100 is prepared from the same kind of softwood dissolving pulp as above. The pulp is carboxymethylated in a chemical pretreatment step and then run once through the microfluidizer.<sup>28</sup>

The DP-1100 sample has the highest average molar mass but also shows some other differences compared with samples based on enzymatic pretreatment. The degree of dispersion of nanofibrils is higher (higher suspension viscosity and more transparent suspension) and the cellulose surface contains carboxylic acid groups due to the chemical pretreatment.<sup>28</sup>

**Preparation of Cellulose Nanopaper.** Cellulose nanopaper films were prepared by vacuum filtration of a 0.2% (by weight) MFC suspension. Prior to filtration, the suspension was stirred for 48 h to ensure well-dispersed nanofibrils. All films, except DP-800, were filtrated on a glass filter funnel (11.5 cm in diameter) using Munktell

filter paper, grade OOH, Munktell Filter AB, Sweden. Films prepared of DP-800 were filtrated on a glass filter funnel (7.2 cm in diameter) using filter membrane, 0.65 μm DVPP, Millipore, U.S.A. After filtration, the wet films were stacked between filter papers and then dried at 55 °C for 48 h at about 10 kPa applied pressure. This resulted in MFC films with thicknesses in the range 60–80 μm.

Porous films are prepared by solvent exchange on the filtered film before drying. After filtration, the wet film was immersed in methanol, ethanol, or acetone for 2 h. The solvent was replaced by fresh solvent and the film was left for another 24 h. Then the film was dried in the same way as described above. This resulted in films of various porosities and thicknesses in the range of 70–90 μm.

In the present study, films are dried from water if nothing else is written.

**Degree of Polymerization and molecular Weight Distribution.** Degree of polymerization was calculated from intrinsic viscosity data,  $\eta$ , using  $\eta = 0.42DP$  for  $DP < 950$  and  $\eta = 2.28DP^{0.76}$  for  $DP > 950$ .<sup>29</sup> The intrinsic viscosity measurements were performed on the pulps according to SCAN-CM 15:99 (which agrees with ISO 5351-1: 1981, option B) with cupriethylenediamine as solvent.<sup>30</sup> Fibers were weighed in the wet state. The water content of the sample was taken into account when adding water to the samples.

The molecular weight distribution was measured by size exclusion chromatography, SEC. The solvent system used was dimethylacetamide (DMAc)/LiCl. Pullulan was used for calibration. A refractive index detector was used. Water was removed from the MFC suspensions by solvent exchange with methanol and DMAc before being dissolved in DMAc/LiCl containing ethylisocyanate.

**Density and Porosity.** An Archimedes scale was used for determination of density for the MFC films. The density was calculated from the displacement for the sample when immersed in mercury.<sup>31</sup> Porosity is calculated from the measured density by eq 1.

$$\text{porosity} = \frac{1 - \rho_f}{\rho_c} \quad (1)$$

where  $\rho_f$  corresponds to the density of the film and  $\rho_c$  corresponds to the density for the cellulose, which is assumed to be 1500 kg/m<sup>3</sup>.

**Field-Emission Scanning Electron Microscopy (FE-SEM).** A Hitachi S-4300 scanning electron microscope, operated at 2 kV, was used to capture secondary electron images of cellulose nanopaper surfaces and cross-sections. The samples were mounted onto a metal substrate using carbon tape and coated with a thin layer of gold.

**X-ray Diffraction.** X-ray diffraction photographs were taken by an imaging plate (IP) having a camera length of 38.3 mm. The Cu Kα radiation, generated with a Rigaku RINT-2000 at 40 kV, 20 mA, was irradiated on the specimen perpendicular or parallel to the film surface.

The crystallite orientation,  $f$ , in the films was determined by calculating the Herman's orientation function<sup>32</sup> for the azimuthal profile of the 200 reflection in the X-ray diffractogram.

$$f = \frac{3\langle \cos^2 \Phi \rangle - 1}{2} \quad (2)$$

$$\langle \cos^2 \Phi \rangle = \frac{\int_0^{\pi/2} I(\Phi) \cos^2 \Phi \sin \Phi d\Phi}{\int_0^{\pi/2} I(\Phi) \sin \Phi d\Phi} \quad (3)$$

where  $I(\Phi)$  is the intensity at the azimuthal angle  $\Phi$ .

**Tensile Test.** Tensile tests of the films were performed with a Universal Materials Testing Machine from Instron, U.S.A., equipped with a 500 N load cell. Specimens of 40 mm length and 60–80 μm thickness and 5 mm width were tested at a cross-head speed of 4 mm/min, which corresponds to an initial strain rate of 10% min<sup>-1</sup>. The relative humidity was kept at 50% and the temperature at 23 °C. The displacement was measured by Digital Speckle Photography (DSP). A pattern was prepared for the DSP by printer toner. During the tensile test, photographs of the whole specimen were captured. The frame rate was set to five frames per second. The results for each material are

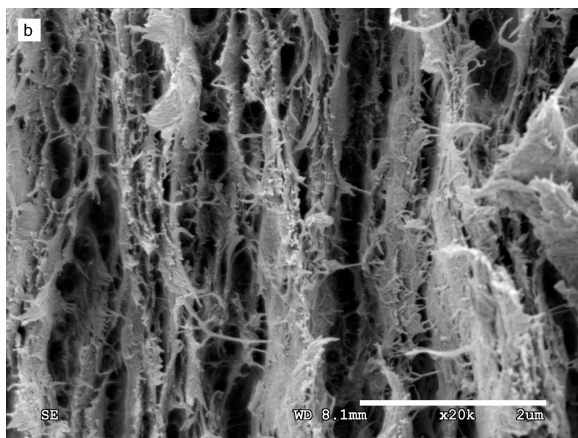
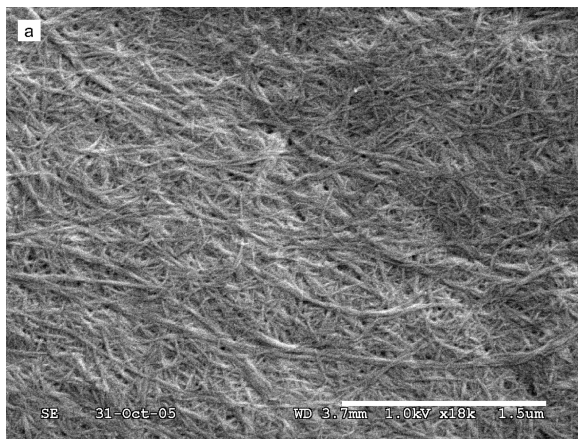


**Figure 1.** FE-SEM micrographs of (a) a cellulose nanofibril film surface showing a fibrous network (scale bar is  $1.5\text{ }\mu\text{m}$ ), (b) the cross section of a fracture surface of a film showing a layered structure (scale bar is  $2\text{ }\mu\text{m}$ ), and (c) a fracture surface viewed perpendicular to the film surface (scale bar is  $1\text{ }\mu\text{m}$ ). These films were dried from water suspension. The film in (a) is prepared from DP-1100 and the other two are prepared from DP-800.

based on at least six specimens, if nothing else is mentioned. Toughness is defined as work to fracture and is calculated as the area under the stress-strain curve.<sup>33</sup> The yield strength,  $\sigma_{0.2}$ , was determined at the intersection of a 0.2% offset line and the stress-strain curve.<sup>34</sup>

**Acoustic Emission.** Acoustic emission (AE) monitoring was used while loading slender specimens in tension to study evolution of the microfracture processes. A MTS servo-hydraulic testing machine was employed, which has been modified to reduce its mechanical noise to better fit AE testing. The geometry of the specimens in all AE experiments was 50 mm (gauge length) and 8 mm (width) and the tests were performed at a displacement rate of 0.5 mm/min. The AE

**Table 1.** Density and Porosity Data as Well as Herman's Orientation Function,  $f$ , Calculated from Diffraction Patterns for Different Films

material	DP	liquid	density [kg/m <sup>3</sup> ]	porosity [%]	$f$ , in the plane of the film	$f$ , out of plane
DP-410	410	water	1200	20		
DP-580	580	water	1140	24		
DP-820	820	water				
DP-1100	1100	water	1080	28	-0.008	-0.17
DP-800	800	water	1215	19	0.002	-0.13
DP-800	800	methanol	1085	28	0.002	-0.14
DP-800	800	ethanol	930	38	0.009	-0.12
DP-800	800	acetone	900	40	0.005	-0.12

sensor is a small, lightweight, piezoelectric resonance frequency sensor from Vallen Systeme GmbH, Germany. The sensor is 3 mm in diameter and encapsulated in a shelter having a diameter of 6 mm.<sup>35</sup> It was positioned in the center point of each specimen and kept in place by a small magnet. Since the resonance frequency of the sensor is around 300 kHz it is unlikely that noise from the testing machine influences AE measurements during the experiments. The AE signals were recorded by a system manufactured by Vallen Systeme GmbH, Germany. The relative humidity was kept at 50% and the temperature was 23 °C.

## Results and Discussion

**Structural Characterization.** Improved understanding of structure–mechanical property relationships in cellulose nanopaper structures is based on proper structural information. In particular, improved understanding is needed of the porous structure and associated “nanopaper” characteristics. In Figure 1a, a surface micrograph of a fibrous nanofibril network film is presented. A fine weblike, and highly fibrous network structure,

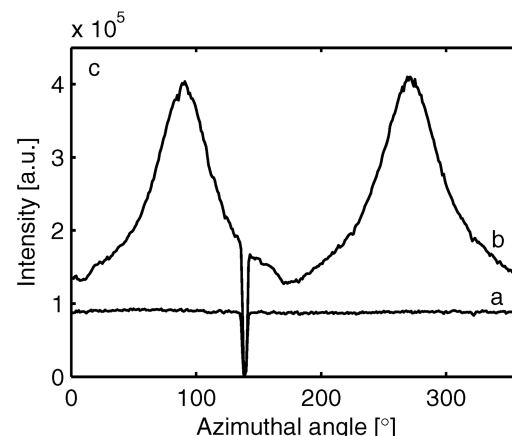
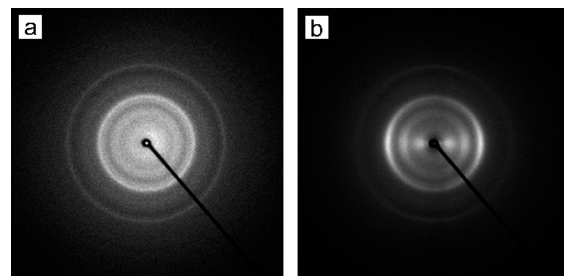


**Figure 2.** X-ray diffractograms perpendicular (a) and parallel (b) to the film surfaces. In (c), the intensity is plotted vs the azimuthal angle for the 200 reflection in (a) and (b). The film was prepared from DP-800, dried from water.

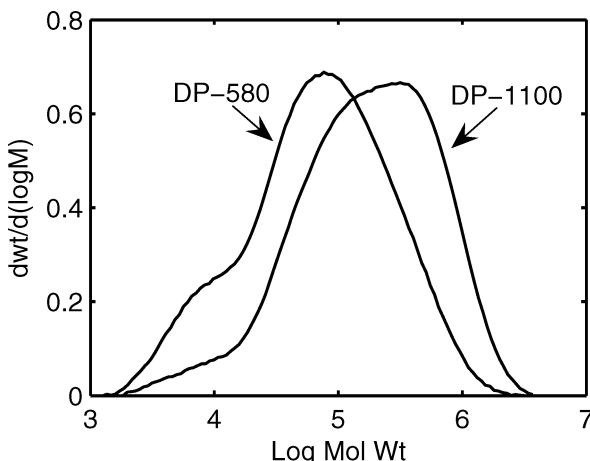


**Figure 3.** Molar mass distribution for MFC DP-580 and DP-1100.

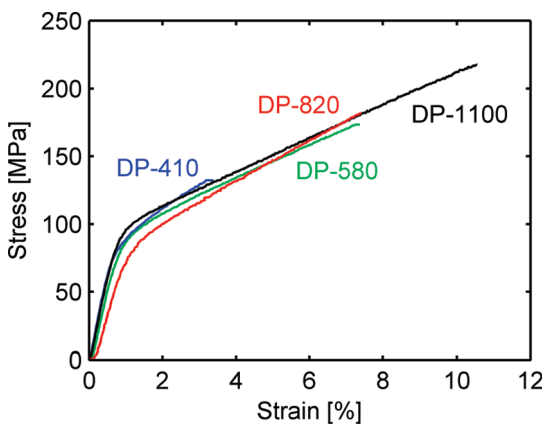


**Figure 4.** Typical stress-strain curves for MFC films prepared of MFC with different DP.

is apparent, consisting of nanofibrils from wood pulp fibers (see Experimental Section). The typical lateral dimension is 10–40 nm. This indicates that the individual nanofibrils most often consist of cellulose microfibril aggregates<sup>36</sup> rather than smaller individual microfibrils. The nanofibril length is several micrometers and nanofibril ends are not apparent. Furthermore, individual nanofibrils are swirled and physically entangled with respect to each other. The predominant orientation appears to be random-in-the-plane. The swirled characteristics are different from the materials based on rod-like tunicate whiskers<sup>4,5</sup> but resembles the structure of parenchyma-based cellulose.<sup>37</sup> Because films were prepared from water suspensions, we expect strong secondary interfibril interaction including hydrogen bonds. This is analogous to the interaction in cast microcrystalline cellulose (MCC).<sup>38</sup> No difference in average nanofibril width could be observed for the different samples studied.

The layered structure is apparent in Figure 1b. Nanofibrils are deposited flatly in swirled conformations on the porous membrane during vacuum filtration. The fibrillar nature of the material is also apparent in the fracture surface presented in Figure 1c, to be discussed later. Perhaps the most important structural characteristic is that the nanofibrillar films are porous. The nature of the porosity and its extent is of obvious significance to physical properties. The pores are irregular in shape, as expected in a high-density network, and a considerable amount of porosity is apparent in Figure 1a. The typical pore diameter is in the range 10–50 nm (Figure 1a). Porosity data are presented in Table 1. The “reference” films prepared from water show porosities as high as 28%. Films dried from the less hydrophilic liquids methanol, ethanol, and acetone show

porosities up to 40%. Yano et al.<sup>20</sup> reported higher densities for films dried from water than the present data, probably due to the higher pressure used during the film consolidation procedure, 100 MPa compared with the present 10 kPa.

Figure 2 presents XRD data perpendicular and parallel to the film surface. The orientation in the plane of the film is completely random, confirming the impression from Figure 1. Data parallel to the film surface show ordering in this plane, although a limited extent of out-of-plane orientation is present (Table 1). In a fiber network mechanics context, increased out-of-plane orientation will lower the in-plane modulus.

The molar mass distribution in the cellulose nanofibrils is an important structural characteristic. Size exclusion chromatography (SEC) data are presented in Figure 3. The sample names are based on the degree of polymerization calculated from intrinsic viscosity data. The DP-580 sample shows a much larger fraction of molecules in the low molar mass region ( $<10^4$ ). Whether this fraction corresponds to a population of shorter microfibrils is unclear, although Battista indeed found a direct correlation between average molar mass and rod length for the case of MCC.<sup>38</sup>

**Stress–Strain Behavior and Deformation Mechanisms.** In Figure 4, the stress–strain behavior in uniaxial tension for cellulose nanofibril networks is presented. Associated property data are provided in Table 2. The behavior is fairly linear up to about 0.5%. At a stress in the region of 90 MPa (apparent yield stress  $\sigma_{0.2}$ ), there is a knee in the curve followed by a linear and fairly strongly strain-hardening region. This region is termed the plastic region based on a phenomenological interpretation. Films of nanofibrils prepared from the same pulp but with different resulting viscosity average molar mass ( $M_v$ ) roughly follow the same curve but show different strain-to-failure  $\epsilon_c$ . Increased average molar mass  $M_v$  leads to higher  $\epsilon_c$  and the associated higher ultimate tensile strength  $\sigma_c$ . In Mark<sup>39</sup> it is pointed out that below a cellulose DP of 2500, the strength of individual plant fiber cells subjected to chemical or thermal treatment depends on cellulose molar mass. Failure is suggested to occur by slippage of the extended cellulose chains rather than by covalent bond breakage expected at high DP.<sup>2,39</sup> The data in Figure 4 show that ultimate strength correlates with cellulose molar mass and indicate that cellulose nanofibrils in the network are fracturing in the second linear region. This is also supported by the apparent presence of fractured nanofibrils on the fracture surface in Figure 1c. The work to fracture,  $W_A$ , of the DP-1100 sample is exceptionally high, see Table 2. Very few materials, in particular not porous ones, show this favorable combination of strength, modulus, and strain-to-failure. Furthermore, the preparation procedure simply involves film formation by de-watering of a nanofibril suspension and is environmentally friendly.

Networks of higher porosity were then prepared by drying the films from less polar solvents using a solvent exchange procedure. Stress–strain curves are presented in Figure 5 and associated material data are presented in Table 3. It is quite remarkable that nanopaper with porosity as high as 40% shows such favorable mechanical behavior. Compared with 19% porosity, average strength is reduced from 205 to 95 MPa and average modulus from 14.7 to 7.4 GPa. The strain-to-failure of this fine nanostructured fibrous network (“nanopaper”) is quite insensitive to the presence of small and homogeneously distributed pores.

The yield phenomenon takes place at about the same strain for all porosities but yield stress depends strongly on porosity. One may speculate that yielding is associated with onset of

**Table 2.** Physical and Average Mechanical Properties for MFC Films Prepared of MFC with Different DP<sup>a</sup>

material	porosity [%]	modulus, <i>E</i> [GPa]	slope in the plastic region, <i>n</i> [GPa]	yield stress, $\sigma_{0.2}$ [MPa]	tensile strength, $\sigma_c$ [MPa]	strain-to-failure, $\epsilon_c$ [%]	work to fracture, $W_A$ [MJ/m <sup>3</sup> ]
DP-410	20	13.7 (0.3)	- <sup>b</sup>	81.5 (4.7)	129 (8.7)	3.3 (0.4)	3.0 (0.5)
DP-580	24	10.7 (1.2)	1.27 (0.13)	83.6 (2.1)	159 (16.4)	6.4 (1.7)	7.1 (2.5)
DP-820		10.4 (0.5)	1.50 (0.07)	83.6 (2.8)	181 (12.7)	7.4 (1.5)	9.1 (2.3)
DP-1100	28	13.2 (0.6)	1.28 (0.16)	92.2 (5.2)	214 (6.8)	10.1 (1.4)	15.1 (1.9)

<sup>a</sup> The values in parentheses are the sample standard deviations. <sup>b</sup> Due to low  $\epsilon_c$ , the plastic region is limited and this value can not be calculated.

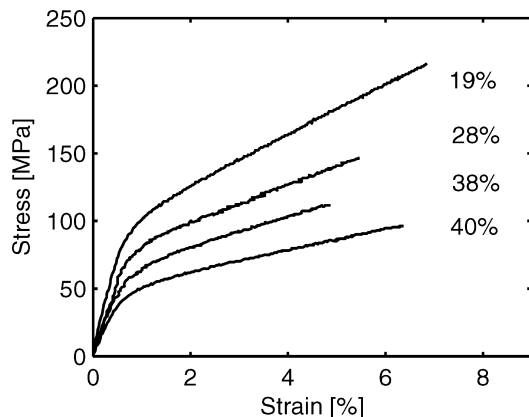


**Figure 5.** Typical stress-strain curves for MFC films with different porosities. For average mechanical properties see Table 3. Cellulose nanofibrils with DP 800 was used.

interfibril debonding and nanofibril slippage facilitated by voids. The lack of molar mass correlation with yield stress indicates that nanofibril fracture is unrelated to the macroscopic yield phenomenon.

The slope *n* in the plastic region also depends on porosity and one may speculate that *n* is related to the frictional resistance to slippage of individual nanofibrils in the network. The slope *n* may also be sensitive to hemicellulose content in the MFC nanofibrils. For instance, the sample with 19% porosity in Table

3 shows the highest *n* (1.82) and is based on the pulp with highest hemicellulose content. In fact, Leopold et al. note that compared with fibers of extremely low hemicellulose content, an increase in hemicellulose content leads to increased pulp fiber strength.<sup>40</sup> He suggests that this is due to improved stress transfer between cellulose crystallites.

The specific modulus of porous networks increases with density, see Figure 6a. There are several possible explanations. The extent of out-of-plane nanofibril orientation may increase with higher network porosity due to the preparation method. This possibility is excluded by the X-ray diffraction data because there is no difference in degree of orientation for samples prepared from different liquids (Table 1). However, in the more porous networks, the interfibril bonds may be weakened by reduced hydrogen-bonding density due to preparation from less hydrophilic liquids. Finally, the relationship between modulus and relative density (relative density is the ratio between the density of the porous material and the density of cellulose, the solid material<sup>41</sup>) is not necessarily linear over a large range of volume fractions (see Figure 6b and consider that Young's modulus = 0 at a relative density of 0). It is likely that nanofibrils are primarily loaded in bending at low relative density and that nanofibril stretching (tension loading) is predominant at high relative density, analogous to the deformation of two-dimensional honeycomb structures.<sup>42,43</sup>

Moisture has a positive effect on the  $\epsilon_c$  of the present films. There is an increase in  $\epsilon_c$  from 2.1% at 0% RH, reported by

**Table 3.** Average Mechanical Properties for Films of Different Porosities<sup>a</sup>

liquid	porosity [%]	modulus, <i>E</i> [GPa]	slope in the plastic region, <i>n</i> [GPa]	yield stress, $\sigma_{0.2}$ [MPa]	tensile strength, $\sigma_c$ [MPa]	strain-to-failure, $\epsilon_c$ [%]	work to fracture, $W_A$ [MJ/m <sup>3</sup> ]
water	19	14.7 (0.5)	1.82 (0.07)	90.6 (3.4)	205 (13) <sup>b</sup>	6.9 (1.2) <sup>b</sup>	9.8 (2.2)
methanol	28	10.8 (1.1)	1.41 (0.07)	75.9 (3.4)	114 (10)	5.4 (1.2)	5.3 (1.5)
ethanol	38	9.3 (0.5)	1.08 (0.06)	57.7 (3.8)	106 (8) <sup>c</sup>	4.7 (0.4) <sup>c</sup>	3.6 (0.5)
acetone	40	7.4 (0.6)	0.83 (0.10)	48.3 (3.4)	95 (8)	6.2 (0.5)	4.2 (0.4)

<sup>a</sup> Cellulose nanofibrils with DP 800 was used. The values in parentheses are the sample standard deviations. <sup>b</sup> Based on four samples. <sup>c</sup> All samples broke close to the grip.

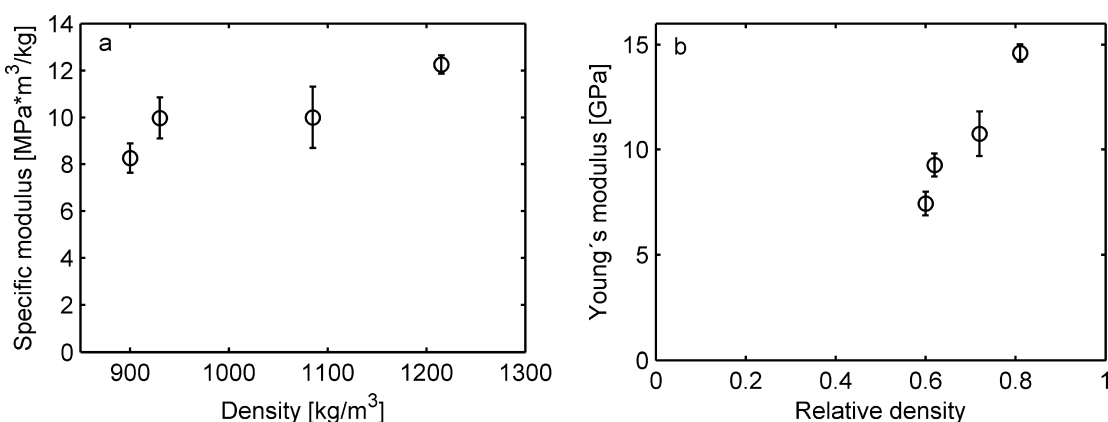


**Figure 6.** Specific modulus vs density (a) and Young's modulus vs relative density (b) for films of different densities (cellulose nanofibrils with DP 800 were used). Relative density is the ratio between the porous material density and the density of cellulose, the solid material, ( $\rho^*/\rho_s$ ) and corresponds to the volume fraction of solid material.<sup>41</sup>

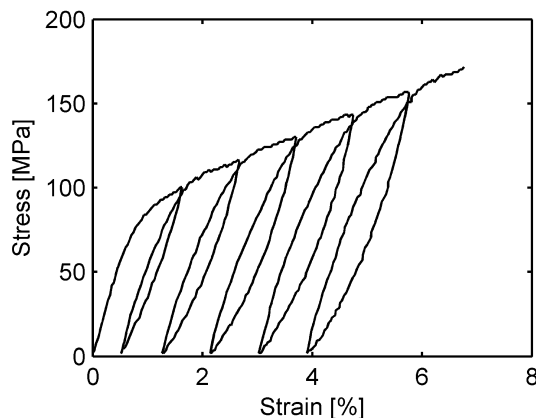


**Figure 7.** Stress–strain data from loading–unloading experiments in uniaxial tension for cellulose nanopaper (DP-1100).

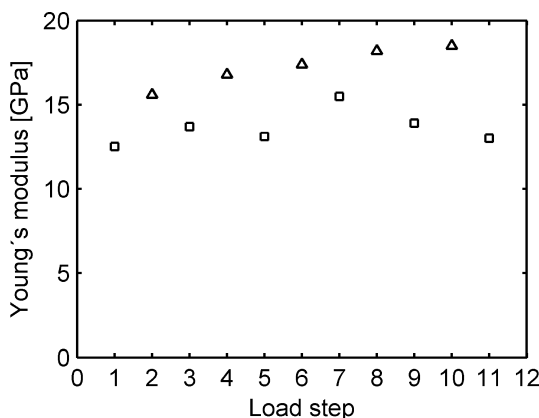
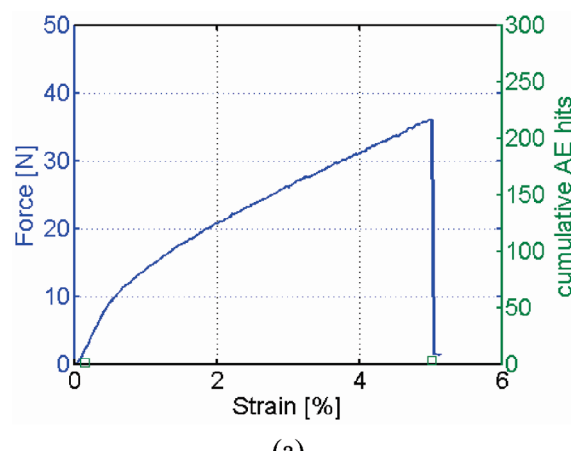


**Figure 8.** Young's modulus as a function of number of loading steps for the cellulose nanopaper specimen tested by loading–unloading in Figure 7; modulus determined during loading (squares) and initial unloading (triangles; DP-1100).

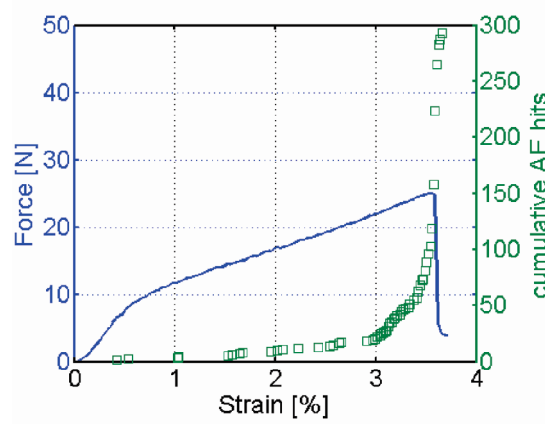
Svagan et al.<sup>17</sup> to 6.9% at 50% RH (DP-800 dried from water). Meanwhile, moisture does not seem to have a strong negative effect on the Young's modulus, 13 GPa at 0% RH,<sup>17</sup> compared with 14.7 GPa at 50% RH.

To examine the nature of the plastic region, repeated loading–unloading experiments are performed. Data confirm the inelastic nature of deformation in this region, see Figure 7. Interestingly, there is a slight increase in modulus with strain, see Figure 8. Many microcomposites show the opposite behavior due to microscopic damage, that is, in the form of debond cracks at the reinforcement–matrix interface.<sup>44</sup> However, so-called “all-cellulose composites”, based on cellulose I crystallites, in a more disordered cellulosic matrix, show similar behavior as the present porous nanofibril network.<sup>45</sup> Gindl suggested that increased modulus is due to deformation-induced reorientation of cellulose crystallites with respect to the loading direction. Keckes<sup>46</sup> reported unchanged stiffness in the plastic range of green wood single fibers of high microfibril angle. This was ascribed to a “stick-slip” mechanism. The mechanism is suggested to involve breakage of “unspecific bonds” at a certain shear stress and associated plastic flow of the wood polymer matrix. Upon unloading, new bonds are formed and new microfibril positions are locked in.

If we assume that the yield phenomenon in the present nanopaper structures is not related to yielding of the nanofibrils themselves, then deformation mechanisms are related to the nanopaper structure. Because the present yield stress is increased by increased number of loading cycles in the plastic range (see



(a)



(b)

**Figure 9.** Force-strain data and acoustic emission events for (a) cellulose nanopaper (DP-800) and (b) conventional paper.

Figure 7), the nanofibril network structure is reorganized as it is deformed beyond yielding. This reorganization increases the yield stress.

Acoustic emission (AE) was registered during loading, and the data are compared with conventional paper in Figure 9. Interestingly, AE measurements on cellulose nanopaper (Figure 9a) result in 3–4 events per test, in contrast with the behavior of conventional paper, where several hundred events are detected (Figure 9b). Apparently, the subcritical failure events in nanopaper (i.e., interfibril debonding, nanofibril plasticity, nanofibril tensile fracture, nanofibril slippage) do not emit sufficient energy to be detected.

## Conclusions

Cellulose nanopaper films were carefully prepared from cellulose nanofibrils in water suspension. The best mechanical properties resulted from high molar mass nanofibrils obtained from carboxymethylation pretreatment of wood pulp fibers followed by mechanical disintegration using a high shear homogenizer. This nanopaper sample shows very high toughness,  $W_A = 15 \text{ MJ/m}^3$ , in uniaxial tension and this is associated with a strain-to-failure as high as 10%. Despite a porosity of 28% for the toughest nanopaper, the Young's modulus (13.2 GPa) and tensile strength (214 MPa) are remarkably high. Cellulose nanopaper is a network composed of intertwined nanofibrils, with an aspect ratio exceeding 100 and with random-in-the-plane nanofibril orientation. The tensile strength, toughness, and strain-to-failure do correlate with average molar mass

$M_v$  of the nanofibrils. This indicates that ultimate failure is associated with nanofibril fracture. The strain-to-failure  $\epsilon_c$  is quite high (around 6%) also at porosities as high as 40%. In addition,  $\epsilon_c$  is fairly insensitive to porosity in the range 20–40%. Most likely, this is due to the small average pore size ( $\approx 10\text{--}50$  nm), homogeneous pore distribution, strong interfibril adhesion, and the nanofibrillar nature and extended chain conformation of the cellulose.

The large  $\epsilon_c$  (10%) at 28% porosity cannot be explained only by irreversible tensile deformation of the nanofibrils themselves. Instead one may speculate that the plastic region is associated with interfibril debonding, nanofibril bending and plasticity, nanofibril slippage, and ultimately, nanofibril tensile fracture. Conventional “micropaper” shows inferior toughness. The superiority of nanopaper is likely to be caused by higher fibril strength, more favorable interfibril adhesion characteristics, and much smaller and more homogeneously distributed defects (i.e., voids). In fact, its renewable resource origin in combination with high toughness and the possibility to tailor porosity makes cellulose nanopaper an interesting candidate in nanotechnology applications of the future.

**Acknowledgment.** Anna Svagan (KTH) and Karin Athley (STFI-Packforsk) are acknowledged for their kind help with density measurements. Mikael Ankerfors (STFI-Packforsk) is acknowledged for kindly providing microfibrillated cellulose.

## References and Notes

- (1) Sakurada, I.; Nukushina, Y.; Ito, T. *J. Polym. Sci.* **1962**, *57*, 651.
- (2) Wainwright, S. A.; Biggs, W. D.; Currey, J. D.; Gosline, J. M. *Mechanical design in organisms*; Princeton University Press: Princeton, NJ, 1982.
- (3) Bledzki, A. K.; Gassan, J. *Prog. Polym. Sci.* **1999**, *24*, 221.
- (4) Favier, V.; Canova, G. R.; Cavaillé, J. Y.; Chanzy, H.; Dufresne, A.; Gauthier, C. *Polym. Adv. Technol.* **1995**, *6*, 351.
- (5) Favier, V.; Chanzy, H.; Cavaillé, J. Y. *Macromolecules* **1995**, *28*, 6365.
- (6) Azizi Samir, M. A. S.; Alloin, F.; Dufresne, A. *Biomacromolecules* **2005**, *6*, 612.
- (7) Berglund, L. A. Cellulose-based nanocomposites. In *Natural Fibers, Biopolymers, and their Biocomposites*; Mohanty, A. K., Misra, M., Drzal, L. T., Eds.; CRC Press: Boca Raton, FL, 2005.
- (8) Nakagaito, A. N.; Yano, H. *Appl. Phys. A: Mater. Sci. Process.* **2005**, *80*, 155.
- (9) Henriksson, M.; Berglund, L. A. *J. Appl. Polym. Sci.* **2007**, *106*, 2817.
- (10) Czaja, W. K.; Young, D. J.; Kawecki, M.; Brown, R. M., Jr. *Biomacromolecules* **2007**, *8*, 1.
- (11) Klemm, D.; Schumann, D.; Udhhardt, U.; Marsch, S. *Prog. Polym. Sci.* **2001**, *26*, 1561.
- (12) Yano, H.; Sugiyama, J.; Nakagaito, A. N.; Nogi, M.; Matsuura, T.; Hikita, M.; Handa, K. *Adv. Mater.* **2005**, *17*, 153.
- (13) Henriksson, M.; Henriksson, G.; Berglund, L. A.; Lindström, T. *Eur. Polym. J.* **2007**, *43*, 3434.
- (14) Pääkkö, M.; Ankerfors, M.; Kosonen, H.; Nykänen, A.; Ahola, S.; Österberg, M.; Ruokolainen, J.; Laine, J.; Larsson, P. T.; Ikkala, O.; Lindström, T. *Biomacromolecules* **2007**, *8*, 1934.
- (15) Herrick, F. W.; Casebier, R. L.; Hamilton, J. K.; Sandberg, K. R. *J. Appl. Polym. Sci.* **1983**, *37*, 797.
- (16) Turbak, A. F.; Snyder, F. W.; Sandberg, K. R. *J. Appl. Polym. Sci.* **1983**, *37*, 815.
- (17) Svagan, A. J.; Azizi Samir, M. A. S.; Berglund, L. A. *Biomacromolecules* **2007**, *8*, 2556.
- (18) Dufresne, A.; Dupeyre, D.; Vignon, M. R. *J. Appl. Polym. Sci.* **2000**, *76*, 2080.
- (19) Taniguchi, T.; Okamura, K. *Polym. Int.* **1998**, *47*, 291.
- (20) Yano, H.; Nakahara, S. *J. Mater. Sci.* **2004**, *39*, 1635.
- (21) Zimmerman, T.; Pöhler, E.; Geiger, T. *Adv. Eng. Mater.* **2004**, *6*, 754.
- (22) Iwamoto, S.; Nakagaito, A. N.; Yano, H. *Appl. Phys. A: Mater. Sci. Process.* **2007**, *89*, 461.
- (23) Dufresne, A.; Cavaille, J. Y.; Vignon, M. R. *J. Appl. Polym. Sci.* **1997**, *64*, 1185.
- (24) Bruce, D. M.; Hobson, R. N.; Farrent, J. W.; Hepworth, D. G. *Composites, Part A* **2005**, *36*, 1486.
- (25) Leitner, J.; Hinterstoisser, B.; Wastyn, M.; Keckes, J.; Gindl, W. *Cellulose* **2007**, *14*, 419.
- (26) Nishi, Y.; Uryu, M.; Yamanaka, S.; Watanabe, K.; Kitamura, N.; Iguchi, M.; Mitsuhashi, S. *J. Mater. Sci.* **1990**, *25*, 2997.
- (27) Nakagaito, A. N.; Iwamoto, S.; Yano, H. *Appl. Phys. A: Mater. Sci. Process.* **2005**, *80*, 93.
- (28) Wågberg, L.; Decher, G.; Norgren, M.; Lindström, T.; Ankerfors, M.; Axnäs, K. *Langmuir* **2008**, *24*, 784–795.
- (29) Marx-Figini, M. *Angew. Makromol. Chem.* **1978**, *72*, 161.
- (30) SCAN-CM 15:99. SCAN Standard. SCAN-test methods are published and recommended by central laboratories for the pulp and paper industry in Denmark, Finland, Norway, and Sweden. They can be obtained from Scandinavian Pulp, Paper and Board Testing Committee, Box 5604, SE-114 86 Stockholm, Sweden.
- (31) Baggerud, E.; Stenström, S.; Lindström, T. Measurement of volume fractions of solid, liquid and gas in kraft and CTMP paper at varying moisture content. In *Proceedings of the International Paper Physics Conference*; TAPPI Press: Atlanta, GA, 2003; pp 157–163.
- (32) Baltá-Calleja, F. J.; Vonk, C. G. *X-ray Scattering of Synthetic Polymers*; Elsevier: Amsterdam, 1989.
- (33) Vogel, S. *Comparative Biomechanics: Life's physical world*; Princeton University Press: NJ, 2003.
- (34) Hertzberg, R. W. *Deformation and fracture mechanics of engineering materials*, 3rd ed.; John Wiley and Sons: New York, 1989.
- (35) Isaksson, P.; Hägglund, R. *Int. J. Solids Struct.* **2007**, *44*, 6135.
- (36) Hult, E. L.; Iversen, T.; Sugiyama, J. *Cellulose* **2003**, *10*, 103.
- (37) Azizi Samir, M. A. S.; Alloin, F.; Paillet, M.; Dufresne, A. *Macromolecules* **2004**, *37*, 4313.
- (38) Battista, O. A. *Microcrystal Polymer Science*; McGraw Hill: NY, 1975.
- (39) Mark, R. E. *Cell wall mechanics of tracheids*; Yale University Press: New Haven, 1967.
- (40) Leopold, B.; McIntosh, D. C. *Tappi* **1961**, *44*, 235.
- (41) Gibson, L. J.; Ashby, M. F. *Cellular solids, structure and properties*, 2nd ed.; Cambridge University Press: Cambridge, 1997.
- (42) Masters, I.; Evans, K. *Compos. Struct.* **1996**, *35*, 403.
- (43) Modén C. S.; Berglund, L. A. *Holzforschung* **2008**, in press.
- (44) Sjögren, B. A.; Berglund, L. A. *Polym. Compos.* **1997**, *18*, 1.
- (45) Gindl, W.; Martinschitz, K. J.; Boesecke, P.; Keckes, J. *Comp. Sci. Tech.* **2006**, *66*, 2639.
- (46) Keckes, J.; Burgert, I.; Frühmann, K.; Müller, M.; Kölln, K.; Hamilton, M.; Burghammer, M.; Roth, S. V.; Stanzl-Tschegg, S.; Fratzl, P. *Nat. Mater.* **2003**, *2*, 810.

BM800038N